THE JOURNAL OF PHYSICAL CHEMISTRY B

pubs.acs.org/JPCB Article

Confinement of Colloids with Competing Interactions in Ordered Porous Materials

Horacio Serna, Eva G. Noya, and Wojciech T. Góźdź*

Cite This: J. Phys. Chem. B 2020, 124, 10567−10577

Read Online

ACCESS | Metrics & More | Article Recommendations

ABSTRACT: In this work, we explore the possibility of promoting the formation of ordered microphases by confinement of colloids with competing interactions in ordered porous materials. For that aim, we consider three families of porous materials modeled as cubic primitive, diamond, and gyroid bicontinuous phases. The structure of the confined colloids is investigated by means of grand canonical Monte Carlo simulations in thermodynamic conditions at which either a cluster crystal or a cylindrical phase is stable in bulk. We find that by tuning the size of the unit cell of these porous materials, numerous novel ordered microphases can be produced, including cluster crystals arranged into close packed and open lattices as well as nonparallel cylindrical phases.

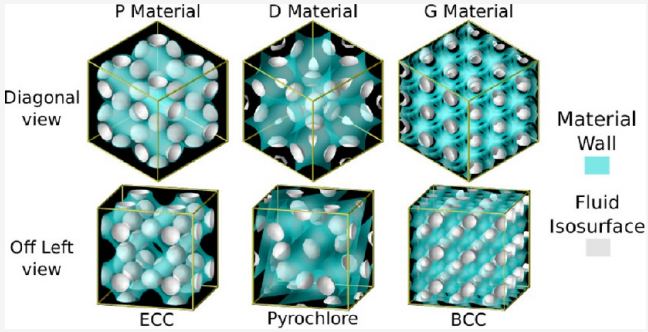

INTRODUCTION

Weakly charged colloidal particles can attract at short distances due to depletion forces and repel at large distances due to screened electrostatic charges.[1,2] Colloidal systems with competing interactions may form ordered microphases in bulk such as crystal-cluster, hexagonal cylindrical, double gyroid, and lamellar phases.[3] Such structures are of interest, both from the theoretical and technological points of view, for example, in bioelectronics, sensor production, drug delivery, and catalysis.[4−6]

Confinement offers an extra parameter to control the behavior of complex colloidal systems. It has been demonstrated in experiments[7−10] and simulations[11−16] that systems with competing interactions under confinement exhibit new thermodynamic as well as structural properties. When confined, several novel structures that are not observed in bulk may be created by tuning the shape of the confining walls.[8,10,12−14,17] An interesting approach to exploit all the possibilities that confinement offers is template-assisted fabrication. On the one hand, this technique has been used to assemble colloidal particles on patterned solid surfaces to create arrays of colloidal aggregates with potential applications on photonics and electronics.[7] On the other hand, it has made use of diblock copolymer self-assembly as a tool to assist the conceptual design of templates with lithographic purposes,[18] to direct the synthesis of nanoparticles while confined within a carbon matrix,[19] and to synthesize mesoporous materials.[20] Typically, these nanofabrication techniques have been applied to bidimensional or quasi-bidimensional systems such as surfaces and thin films, unlike the templating processes within three-dimensional confinement that are still to be explored in more detail.

In this paper, we present an extensive simulation study of colloidal particles with competing interactions confined into periodic porous matrices. Interactions between colloidal particles are modeled via a short-range attractive and long-range repulsive potential (SALR) in the form of a square-well-linear function.[3] We investigate the effect of topology and geometry of the porous material on the formation of ordered structures composed of clusters of colloidal particles by varying the chemical potential (μ) in the range where cluster crystal and cylindrical phases are typically observed in bulk.[3]

In the first section, we present the model and the techniques used for the simulation study. In the second section, we present and analyze the results, and finally, in the third section, we conclude and give some perspectives for future research.

THE MODEL AND THE SIMULATION METHOD

Colloidal particles with SALR interactions are modeled using the square-well-linear potential, consisting of a hard core, an attractive square-well, and a repulsive ramp

Received: September 7, 2020
Revised: October 21, 2020
Published: November 3, 2020

https://dx.doi.org/10.1021/acs.jpcb.0c08148
J. Phys. Chem. B 2020, 124, 10567−10577

$$u_{\mathrm{SALR}}(r_{ij}) = \begin{cases} \infty, & r_{ij} \le \sigma \\ -\varepsilon, & \sigma < r_{ij} \le \lambda\sigma \\ \zeta\varepsilon(\kappa - r_{ij}/\sigma), & \lambda\sigma < r_{ij} \le \kappa\sigma \\ 0, & r_{ij} > \kappa\sigma \end{cases} \quad (1)$$

Here, r_{ij} denotes the distance between particles i and j, λ is the attraction range, κ is the repulsion range, ζ is the the repulsion strength, σ is the diameter of the colloidal particles, and ε is the depth of the energy well.[21] These model parameters were assigned the values $\zeta = 0.05$, $\lambda = 1.5$, and $\kappa = 4$ because the bulk phase diagram is known for this set of model parameters.[3] We are convinced that the behavior of different systems with competing interactions is universal and the specific details in the interaction potential do not matter much. The same qualitative phase behavior can be obtained for systems modeled by the combination of Lennard-Jones and Yukawa potentials with the appropriate choice of parameters. Each choice of the parameters can be associated with some experimental system. It is known that the attractive range of the potential for colloidal systems[22−24] is relatively small compared with the attractive range in the potential studied by us. We anticipate that even for such a small attractive range, the behavior will be still the same. Nevertheless, colloidal systems are not the only systems with competing interactions. For example, block copolymers exhibit very similar phase behavior. In the case of copolymers, there is much more freedom to tune the attractive and repulsive ranges of the interaction potential. Thus, for copolymers, it is easier to construct the experimental systems with the interaction potential studied by us. In this work, our main intention is showing new physical phenomena that can be observed in such systems.

We consider porous materials with structures of cubic bicontinuous phases that can be formed from diblock copolymers, lipid−water, and oil−water-surfactant mixtures. Bicontinuous phases can be used as templates for production of porous materials with ordered well-defined structures. Mathematical models of porous materials with the structure of simple cubic (primitive, P), diamond (D), and gyroid (G) phases can be obtained by using the following expressions[25]

$$\Psi_{\mathrm{P}}(x, y, z) = \cos\left(\frac{2\pi n}{L}x\right) + \cos\left(\frac{2\pi n}{L}y\right) + \cos\left(\frac{2\pi n}{L}z\right) \quad (2)$$

$$\Psi_{\mathrm{D}}(x, y, z) = \cos\left(\frac{2\pi n}{L}(x - y)\right)\cos\left(\frac{2\pi n}{L}z\right) + \sin\left(\frac{2\pi n}{L}(x + y)\right)\sin\left(\frac{2\pi n}{L}z\right) \quad (3)$$

$$\Psi_{\mathrm{G}}(x, y, z) = \sin\left(\frac{2\pi n}{L}x\right)\cos\left(\frac{2\pi n}{L}y\right) + \sin\left(\frac{2\pi n}{L}y\right)\cos\left(\frac{2\pi n}{L}z\right) + \sin\left(\frac{2\pi n}{L}z\right)\cos\left(\frac{2\pi n}{L}x\right) \quad (4)$$

where x, y, and z are the Cartesian coordinates, L is the length of the simulation box edges, and n is the number of unit elements that fit along one axis in the interval $[0, L]$. In Figure 1, we show the shape and topology of the porous materials with the help of the isosurfaces plotted for the equations $\Psi_\alpha(x, y, z) = 0$, where α denotes P, D, and G. Note that the structures of these regular porous materials can be characterized by the number of approximately cylindrical pores that meet in the same region. For the simple cubic structure, this number is six, for diamond, this is four, and for the gyroid, this is three.

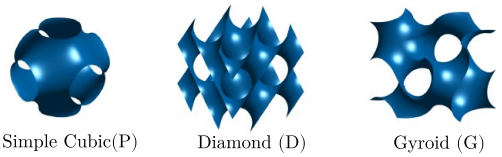

Figure 1. Structures of the porous materials. The surface describes the boundary of the pores defined by eqs 2−4.

The external potential resulting from the presence of the porous material and acting on the colloidal particles is defined as follows

$$\mathcal{V}(r_i) = \begin{cases} \infty, & \Psi_\alpha(r_i) \ge 0 \\ 0, & \Psi_\alpha(r_i) < 0 \end{cases} \quad (5)$$

By locating the pore walls at the points of the isosurface $\Psi_\alpha(x, y, z) = 0$, the bicontinuous porous materials divide the simulation box in two regions of identical volume: one of them can be occupied by the adsorbed fluid particles, while the other region represents the impenetrable porous material. We calculate the number density as $\rho = N/L^3$.

The total energy of the system is thus given by

$$U_{\mathrm{tot}} = \sum_{i=1}^{N-1}\sum_{j>i}^{N} u_{\mathrm{SALR}}(r_{ij}) + \sum_{i=1}^{N}\mathcal{V}(r_i) \quad (6)$$

where N is the total number of colloidal particles.

The structure of the SALR fluid confined in these porous materials was investigated by Monte Carlo simulations in the grand canonical ensemble (μVT). All the magnitudes (chemical potential, temperature, internal energy, density, and distance) are reported using the values σ and ε as units of distance and energy, respectively. Simulations were performed at temperature $T = 0.35$ and at values of chemical potential in the range $-2.65 \le \mu \le -2.10$. In these thermodynamic conditions, the face-centered cubic (FCC) cluster crystal and triangular cylindrical phases are stable in bulk.[3] Periodic boundary conditions are applied along the three directions of space. The size of the pores can be modified by varying the number of unit cells enclosed in the simulation box, i.e., assigning different integer values to n in eqs 2−4. For a given value of L, the pore size adopts discreet values that depend on the integer number n. Different system sizes were considered within the range $L = 20 - 25\sigma$, varying also the number of unit cells n. As our main interest is to promote the formation of ordered cluster structures, results are only reported for those combinations of L and n for which the confined fluid managed to form that type of structure.

Different equilibration times were used in each case depending, mainly, on the system size. Averages were taken over 4×10^9 Monte Carlo steps, from which 4×10^5 independent configurations were taken for calculating the local density. A Monte Carlo step is defined as a trial move that may be a displacement, addition, or deletion of a particle.

The structure of the cluster crystals was identified by measuring several structural properties. Density maps were used to plot density isosurfaces that allow the visualization of

https://dx.doi.org/10.1021/acs.jpcb.0c08148
J. Phys. Chem. B 2020, 124, 10567−10577

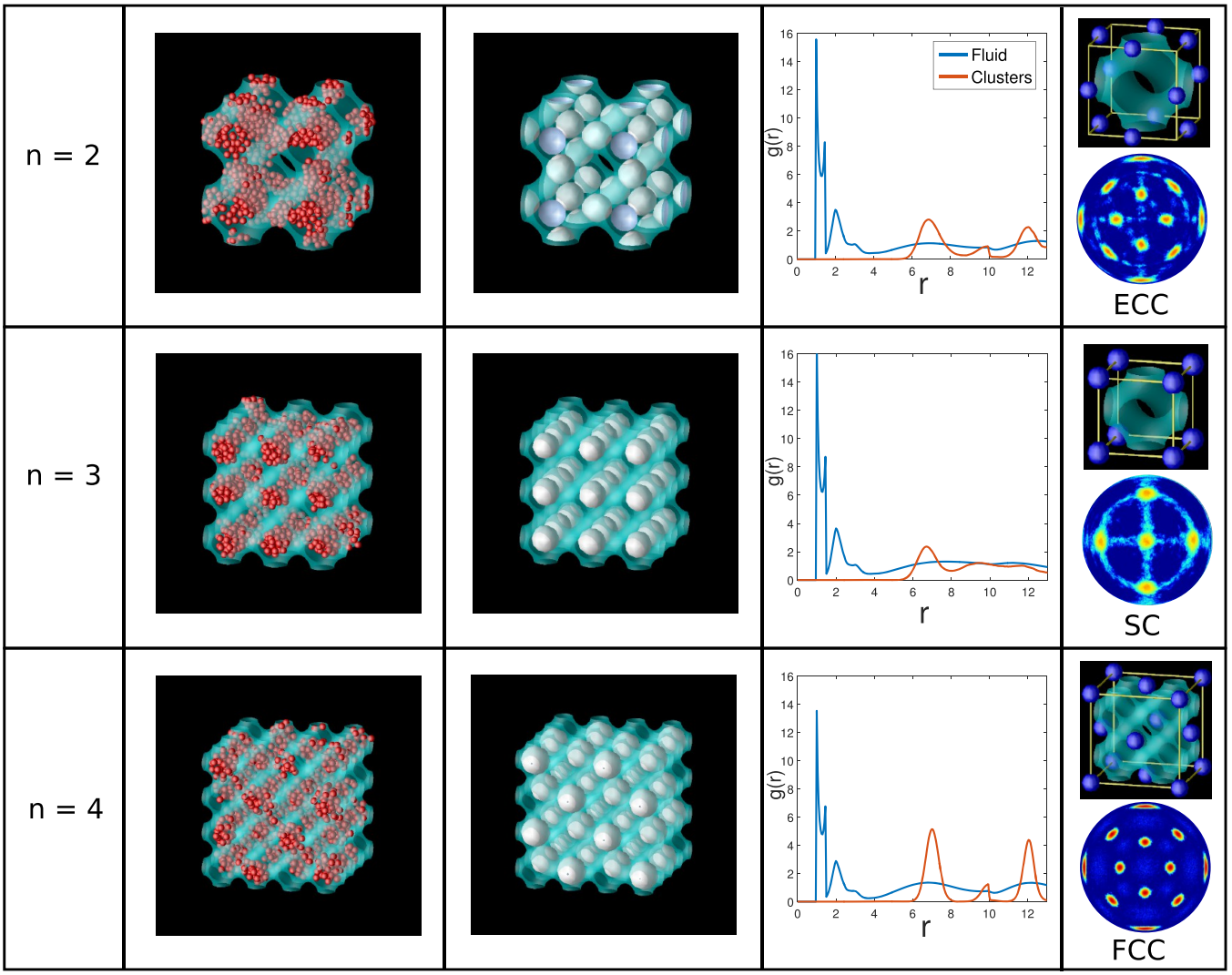

Figure 2. Structures of the SALR fluid confined in the porous material modeled as a primitive bicontinuous surface of edge length $L = 20\sigma$ and different pore sizes n. Simulations were performed in conditions at which the FCC cluster crystal is the stable phase in bulk ($T = 0.35$, $\mu = -2.40$). The value of n is specified in the first column, the second column shows a snapshot of an equilibrium configuration, and the third column shows the local density of the confined fluid. The gray surface corresponds to the isosurface with local density $\rho_{iso} = 0.4$, and the light blue surface corresponds to the pore walls. The average densities are $<\rho> = 0.1055(4),0.1199(9),0.1259(3)$ and the average numbers of particles are $<N> = 844(3),959(7),1007(3)$ for $n = 2,3,4$, respectively. The fourth column shows the particle−particle and cluster−cluster pair correlation functions. In the fifth column, the cluster crystal unit cells and Bond Orientational Order Diagram (BOOD), calculated using the centers of mass of the clusters, are depicted.

the cluster shape and position. Clusters were also identified using a cluster search algorithm,[26] adopting the convention that two particles are bonded and thus belong to the same cluster if the distance between them is lower than the attractive interaction range $\lambda\sigma$. Besides calculating the particle−particle radial distribution function, we also calculated the cluster−cluster distribution function using the center of mass of the clusters. This distribution function allows us to better observe the superstructure formed by the clusters. Both distribution functions were calculated up to a distance equal to half the diagonal of the cubic simulation box, rather to half the edge length as usual.[27,28] Finally, we also calculate bond orientational order diagrams. These diagrams are calculated by projecting the bonds formed by the clusters and its first coordination shell on a unit sphere. The centers of mass of the clusters were used for the evaluation of the BOOD, and the first coordination shell was defined as those clusters that are at a distance shorter than the first minimum in the cluster−cluster distribution function. The unit sphere was then projected in a plane using the area preserving Lambert projection for easier visualization. Different crystal structures are characterized by different BOOD, and thus, it is quite common to use these diagrams in crystal structure identification.[29]

RESULTS

Our goal is to investigate how the process of self-assembly of colloidal cluster crystals is influenced by confinement in ordered porous materials. In particular, we are interested in studying the influence of the topology, symmetry, and geometry of the porous material on the formation of ordered structures that are not encountered in bulk. For that aim, we investigate the structures that adopted the confined fluids on several models of porous materials with structures similar to

https://dx.doi.org/10.1021/acs.jpcb.0c08148
J. Phys. Chem. B 2020, 124, 10567−10577

those of water channels in cubic primitive, diamond, and gyroid phases.[30]

Confinement in the P Material. We start by presenting the results for the simple cubic porous material (see Figure 1, eq 2), which is the one with the simplest network of pores considered in this work. Its porous structure can be described as a collection of approximately spherical cavities arranged in a simple cubic lattice, which are connected by necks somewhat narrower than the spherical cavities. The sizes of the cavities and necks can be modified by changing the number of unit cells, n, which are accommodated in a cubic box of constant edge length L. The diameter of spherical cavities is given by the lattice constant $D_{sphere} = L/n$, whereas that of the cross section of the necks can be approximated as $D_{neck} \approx 3/5D_{sphere}$. In our study, we generated three porous structures by placing $n = 2$, 3, and 4 unit cells in a box of length $L = 20\sigma$ (i.e., 5 times the range of the intermolecular potential, 4σ). The diameters of the spherical cavities in these structures are $D_{sphere}/\sigma = 10.0$, 6.667, and 5.0, whereas the diameters of the cross section of the connecting necks are $D_{neck}/\sigma = 6.0$, 4.0, and 3.0, respectively. For these three porous structures, we investigated the behavior of the confined SALR fluid at $\mu = -2.40$ and $T = 0.35$. In these conditions, the FCC cluster crystal is the stable phase in bulk.[3]

As can be seen in Figure 2, the size and distance between pores play a significant role in the arrangement of the confined SALR fluid. In this figure, we show two different views of the structures formed, as well as the particle−particle and cluster−cluster distribution function and BOOD used for identification of the unit lattice, also shown. In the three cases, SALR particles form spherical clusters (as in bulk), but the spatial distribution of the clusters changes depending on the size and distance between pores. Interestingly, the cluster size does not change much with n. In the three cases, the cluster radius is $r_0 \approx 1.92\sigma$ (measured from local density plots at $\rho_{iso} = 0.4$). This means that in these porous structures, the cluster size is mainly determined by the intermolecular potential rather than from the pore geometry.

In the system with the largest cavities ($n = 2$), clusters sit preferentially at the necks. The distance between nearest spherical cavities is too large (10σ) so that placing the clusters in the spherical cavities would lead to a low density phase. It is possible to obtain a better packed ordered structure occupying instead the necks, for which the distance between nearest neighbor sites is 7.071σ (Figure 2). In this structure, designated as the edge-centered-cubic crystal (ECC), clusters are located at the midpoints of the bonds of a simple cubic lattice. The ECC has eight neighbors in the first coordination shell at a distance $(\sqrt{2}/2)L/n = 0.707L/n$ and six neighbors in the second shell at distance L/n. The BOOD calculated up to the first coordination shell exhibits 12 bright peaks, instead of eight, as one would expect from the number of neighbors in the first coordination shell. The reason is that there are two local orientations of nearest neighbors in this structure.

For slightly smaller pores, $n = 3$, the clusters are located inside the spherical cavities (exactly one cluster in each cavity) and form a simple cubic crystal (SC). In this case, the distance between necks (4.71σ) is too small to avoid repulsion between neighbor clusters located at these sites. The distance between spherical cavities (6.67σ), instead, allows the system to avoid repulsion between nearest clusters and also a fairly efficient packing. The six bright regions in the BOOD are fully compatible with the first coordination shell of the SC lattice. The SC cluster crystal is unstable in bulk for the model considered in this work; however, our results indicate that it can be stabilized inside a porous material. Besides the calculations for $L = 20$ and $n = 3$, we checked the finite size effects repeating the simulations for two additional cases: $L = 13.33$, $n = 2$ and $L = 26.677$, $n = 4$. With this choice of parameters, we maintain the same size of the periodic element of the porous material. We have obtained in all three cases the spherical clusters arranged in the same way. It allows us to conclude that the size of the system does not influence the ordering of the clusters in the porous material.

If the size of the pores is further reduced by setting $n = 4$, the clusters are still located inside the spherical cavities but not all of them are occupied. The distance between the centers of the cavities (5σ) becomes too short to enable full occupation. Thus, only alternate spherical cavities host a cluster, forming a face-centered-cubic (FCC) lattice, which is the stable phase in bulk.[3] The distance between nearest filled spherical cavities in this case is 8.66σ, large enough to avoid a large repulsion between nearest neighbor clusters. The BOOD shows 12 bright regions distributed on the sphere in the way expected for an FCC lattice.[29] Actually, the BOODs of the ECC and the FCC look quite similar, which is due to the structural similarity between these two lattices. The structure of the FCC-shifted half lattice constant resembles the ECC's but with an additional cluster in the center of the unit cell. Note that the FCC cluster crystal is the one exhibiting a cleaner BOOD, with a lower probability of finding neighbor clusters outside the expected orientation in the FCC lattice. We attribute this to the fact that, whereas in the two previous cases, the occupied sites were directly connected to each other, this is no longer true in this porous structure.

The cluster−cluster pair distributions in these three structures (ECC, SC, and FCC) are somewhat similar, with the first two peaks appearing at similar distances. This is expected because the ratio between distances of the first and second coordination shells is the same in the three structures $(1/\sqrt{2})$. The difference between them relies on the number of particles in these two first shells: the ECC has eight first neighbors and six second neighbors, the SC has six first neighbors and twelve second neighbors, and the FCC has twelve first neighbors and six second neighbors. This is consistent with our results, with the FCC exhibiting the stronger first peak and SC exhibiting the weaker first peak. Another common feature of the three cluster crystals is that peaks in the cluster−cluster pair distribution function, especially the first one, are quite broad, indicating that the clusters have quite the freedom to move within the cavities in which they are hosted.

Finally, it is interesting to note that the particle−particle pair correlation function of the fluid is fairly similar for all the crystals, which means that the local structure of the fluid is the same in all cases.

Next, we investigated the structures formed at the same temperature ($T = 0.35$) but at a higher chemical potential, $\mu = -2.10$, at which a hexagonal phase of cylindrical clusters is stable in bulk.[3] The results of the simulations are presented in Figure 3. In these conditions, the confined SALR fluid forms both cylindrical and spherical clusters despite the fact that cluster phases are not stable in bulk.

For the size of the pores set by $n = 3$, only cylindrical clusters are formed. These cylinders are arranged into layers, in which cylindrical clusters are parallel but are stacked randomly so that

https://dx.doi.org/10.1021/acs.jpcb.0c08148
J. Phys. Chem. B 2020, 124, 10567−10577

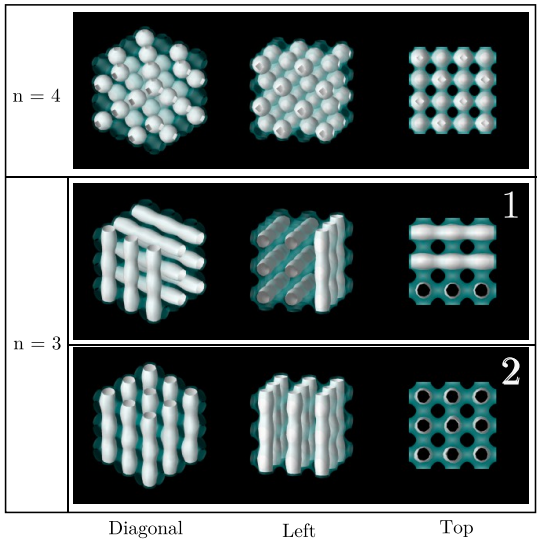

Figure 3. Structures of the SALR fluid confined in the primitive porous material in conditions at which the hexagonal arrangement of cylindrical clusters is the stable phase in bulk ($\mu = -2.10$ and $T = 0.35$). The length of the simulation box edge is $L = 20\sigma$. The gray surface corresponds to the isosurface with local density $\rho_{iso} = 0.4$, and the light blue surface corresponds to the pore walls. The average densities are $<\rho> = 0.1669(4),0.1836(8),0.1842(8)$ and the average numbers of particles are $<N> = 1335(3),1469(7),1474(6)$ for $n = 4,3$, respectively. Three views are shown for each structure. For $n = 4$, an FCC cluster crystal is obtained.

adjacent layers might be oriented parallel or perpendicular to each other (see Figure 3). With the range of the pair potential equal to 4σ, we may expect that interactions between the molecules belonging to adjacent cylindrical clusters (located in channels separated by a distance of $L/n = 6.667\sigma$) are not significant. Note that the equilibrium separation distance between nearest cylinders in the bulk triangular phase is appreciably smaller ($L_{eq} = 6.20\sigma$) than that in the confined structure. Configurations with cylinders oriented parallel and perpendicular to each other in adjacent layers seem to have comparable stability. Both the average energy and density are almost identical in any of those configurations shown in Figure 3. For $n = 3$, the average energy and density are (1) $<u> = -3.2949$ and $<\rho> = 0.1836$ and (2) $<u> = -3.2925$ and $<\rho> = 0.1842$. The radius of the cylindrical clusters is $r_0 \approx 1.68\sigma$, very close to the bulk equilibrium radius of the cylindrical phase under the same thermodynamic conditions $r_{eq} = 1.70\sigma$.

For the size of the pores defined by $n = 4$, the confined fluid does no longer form cylindrical clusters as in bulk. Instead, we observe the nucleation of spherical clusters of radius $r_0 \approx 2.17\sigma$, slightly larger than the radius of the clusters found at lower chemical potential in the primitive porous material, at the three considered porous sizes (Figure 2). The size of the bottlenecks that link the cavities of the porous network ($D_{neck} \approx 3\sigma$) is not large enough to host straight cylinders of radius comparable to those obtained for $n = 3$. Thus, cylinders could only fit in these channels if they exhibited periodic narrowings at the necks. In this situation, the confined fluid prefers to organize again into nearly spherical clusters, arranged in the FCC lattice similar to the behavior observed at a lower

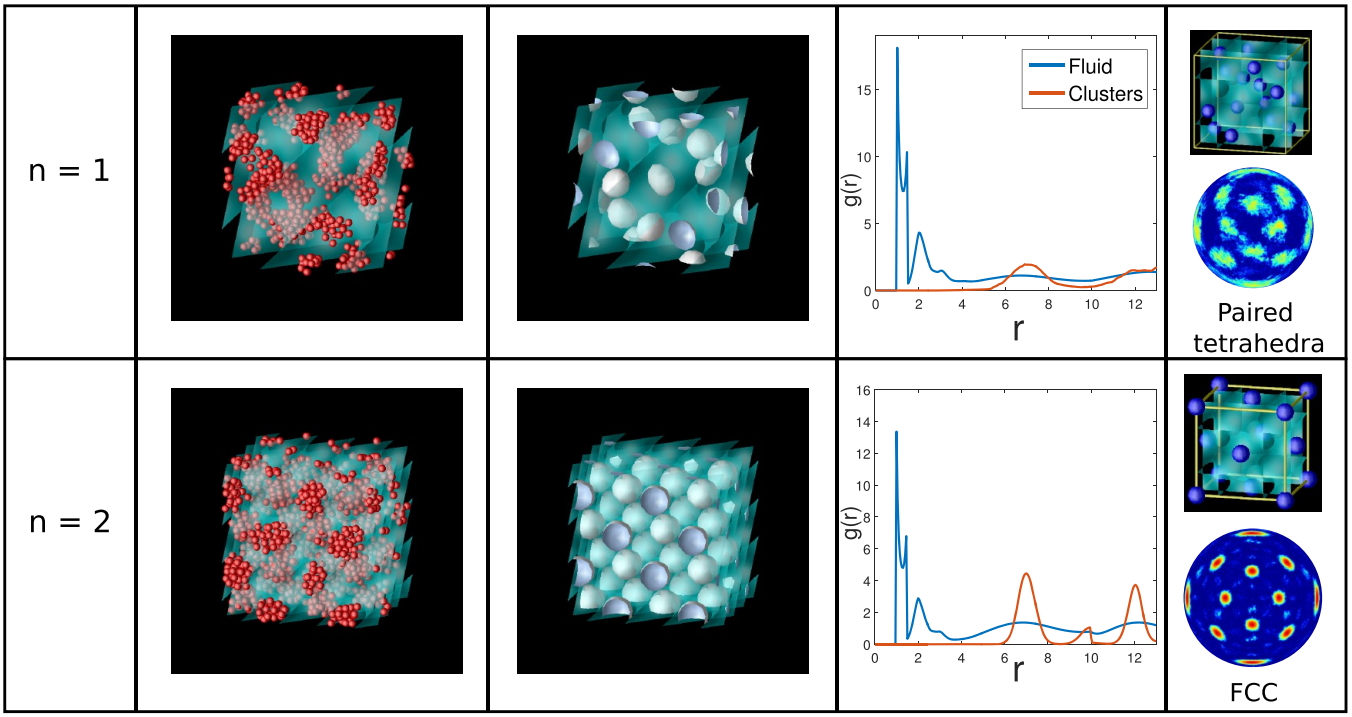

Figure 4. Structures of a confined SALR fluid in porous materials with a diamond structure at $T = 0.35$ and $\mu = -2.40$, conditions at which the FCC cluster crystal is the stable phase in bulk. The length of the simulation box edge is $L = 20\sigma$. In the second column, a snapshot of an equilibrium configuration is shown, and in the third one, the local density is presented. The gray surface corresponds to the isosurface with local density $\rho_{iso} = 0.4$, and the light blue surface correspond to the pore walls. The average densities are $<\rho> = 0.0884(8),0.1301(3)$ and the average numbers of particles are $<N> = 707(7),1041(3)$ for $n = 1,2$, respectively. The fourth column shows the particle−particle and cluster−cluster pair correlation functions, whereas the fifth column shows the unit cell and BOOD calculated using the clusters' centers of mass.

https://dx.doi.org/10.1021/acs.jpcb.0c08148
J. Phys. Chem. B 2020, 124, 10567−10577

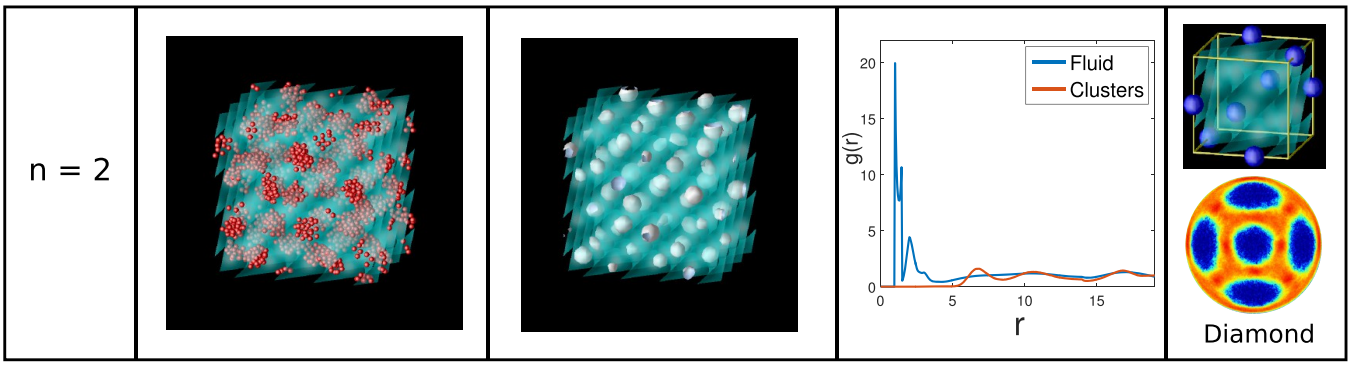

Figure 5. Structure of a confined SALR fluid in a porous material with a diamond structure at $T = 0.35$ and $\mu = -2.48$, conditions at which the FCC cluster crystal is the stable phase in bulk. The length of the simulation box edge, $L = 28\sigma$ with $n = 2$, was chosen to promote the formation of a diamond cluster crystal. In the second column, a snapshot of an equilibrium configuration is shown, and in the third one, the local density is presented. The gray surface corresponds to the isosurface with local density $\rho_{iso} = 0.4$, and the light blue surface corresponds to the pore walls. The average density is $<\rho> = 0.08386(146)$, and the average number of particles is $<N> = 1840(32)$. The fourth column shows the particle−particle and cluster−cluster pair correlation functions, whereas the fifth column shows the unit cell and BOOD calculated using the clusters' centers of mass.

chemical potential. The fact that the FCC crystal is able to survive up to higher chemical potentials than in bulk is evidence of the high stability of this crystal but also of the phase diagram shift experienced by fluids under confinement.[15,16]

Confinement in the D Material. Next, we focus on the diamond porous structure. Let us start by discussing the assembly behavior for pore sizes obtained by setting $L = 20\sigma$ and varying the number of unit cells n. Simulations were performed at $T = 0.35$ and $\mu = -2.40$, i.e., the same thermodynamic conditions used in the first study with the primitive structure and for which the FCC cluster crystal is the stable phase in bulk. In this case, ordered cluster structures were obtained for the porous materials with $n = 1$ and 2 (see Figure 4). For $n = 1$, the spherical clusters are located at the midpoint of the pores that connect adjacent diamond lattice sites, with an analogous behavior to that found for the primitive porous matrix with $L = 20$ and $n = 2$. In the diamond matrix, the distance between the nearest lattice sites is $D_{sphere} = \sqrt{3}/4 \times L/n = 8.667 \times L/n$ and that between the midpoints of the connecting pores is $D_{neck} = \sqrt{2}/4 \times L/n = 7.071 \times L/n$. For $n = 1$, the distance between nearest connecting pores allows the system to avoid repulsion between clusters and a more efficient packing than occupying the lattice nodes. As a consequence, the clusters organize into the pyrochlore crystal structure, which results from full occupation of the pores connecting the diamond lattice sites. This crystal structure has been previously observed in silicate compounds (high cristobalite), in triblock Janus particles,[31,32] and in a repulsive square shoulder isotropic model.[33]

For $n = 2$, the distance between the diamond lattice sites becomes $D_{sphere} = 4.33\sigma$ and that between the pores connecting these sites is $D_{neck} = 3.52\sigma$. Both distances are too small to avoid repulsion between clusters hosted in either of these two types of sites. The solution that the system finds is to occupy the second neighbor cavities of the diamond pore structure separated by a distance $\sqrt{2}/2 \times L/n = 7.071$, forming an FCC structure. Note that a diamond lattice can also be viewed as two interpenetrated FCC lattices displaced a distance $(L/n)/4$ along the diagonal of the cube. The resulting FCC lattice is obtained by occupying only one of these two interpenetrated lattices.

The pair distribution functions of these two cluster crystals are shown in Figure 4. The particle−particle distribution functions are very similar for the two values of n and for the cluster crystal obtained with the primitive porous system. However, the cluster−cluster distribution functions are clearly different, evidencing the different structural arrangement of the clusters. The pyrochlore structure has six neighbors in the first coordination shell and twelve on the second one, with the second shell appearing at a distance $3/\sqrt{3}$ larger than the first shell in a perfect lattice. This is consistent with the cluster−cluster distribution function whose first and second peaks appear at distances 7σ and 12σ, approximately. The cluster−cluster pair distribution of the fluid confined in the material with $n = 2$ instead shows peaks at distances 7σ and 10σ, with a ratio between the two distances close to the value $\sqrt{2}$, corresponding to a perfect FCC lattice. The BOOD diagram displays 12 bright spots in both cases that are blurry in the pyrochlore lattice and quite sharp in the FCC lattice. The reason why there are 12 bright spots in the BOOD diagram of the pyrochlore structure is again because, although there are six neighbors in the first coordination shell, they can be found in two different orientations in the crystal. Note that the FCC structure found in the primitive porous material also exhibited sharper peaks, as compared to the other formed cluster crystals. As in that case, this can be reflecting that not only the FCC cluster crystal is the stable phase in bulk but also that the occupied sites in the porous materials when the FCC is formed are not connected directly to each other.

At this point, we found it somewhat surprising that the SALR fluid did not manage to assemble into a diamond cluster crystal when confined in a porous material with a diamond structure. One would expect that this porous matrix would act as a mold to promote the formation of the diamond cluster crystal. However, the confined fluid prefers to organize into other ordered structures. One possible reason for not obtaining the diamond cluster crystal is that the dimensions of the porous material were not chosen appropriately to favor its formation. Reviewing the cluster crystals obtained so far for the P and D lattices in thermodynamic conditions at which the FCC cluster crystal is the stable phase in bulk, one can identify

https://dx.doi.org/10.1021/acs.jpcb.0c08148
J. Phys. Chem. B 2020, 124, 10567−10577

two common features in these examples: the spherical clusters exhibit roughly the same size (with a diameter of about 1.92σ measured from the isosurface of density $\rho_{iso} = 0.4$), and the interdistance between nearest clusters is within the interval $6.7-8.6\sigma$ that guarantees that repulsion between clusters is small. The distance between lattice points in the system with $n = 1$ falls within the upper limit of this range, but a higher density structure is obtained by occupying the midpoints of the pores connecting adjacent diamond lattice sites. On the other hand, in the porous material obtained with $n = 2$, the distance between lattice points becomes too short so that repulsion between clusters located at those sites is expected to be significant. Thus, we decided to change the size of the unit cell by modifying the length of the box edge within the interval $L = 13 - 17\sigma$, keeping the value of $n = 1$ constant. The distance between nearest diamond sites in porous systems with these dimensions ranges from 5.6 to 7.36σ, and that between the midpoints of nearest connecting pores goes from 4.95 to 6.01σ. These values are, in principle, compatible with the formation of the diamond cluster crystal, and simulations confirmed its appearance for systems with $L = 13.5-16$ and $n = 1$. Once we identified the appropriate unit cell dimensions, we doubled the system size (with edge length $2L$ and setting $n = 2$, so that the unit cell dimensions remain constant) to see if the results were affected by finite size effects. As can be seen in Figure 5, in this bigger system, the fluid organizes on average into a diamond crystal, but the clusters are quite mobile and often adopt fairly elongated shapes. Still, the diamond lattice is clearly distinguished in the density maps, and the measured cluster−cluster pair distribution function and BOOD are compatible with those of diamond. Diamond has four particles in the first coordination shell at distance $\sqrt{3}/4L/n$ and twelve in the second shell at $1/\sqrt{2}L/n$. The BOOD of perfect diamond exhibits eight bright peaks as a result of two possible orientations of the first shell in the crystal. In our case, those eight peaks are visible but are connected to each other by regions of fairly large probability that evidence the high mobility of the clusters. Clusters often leave the lattice node sites, occupying also the connecting pores of the D material. A possible reason why the diamond cluster crystal exhibits fewer defects in the smaller system containing one single unit cell is that this small system might be overconstrained, artificially favoring the formation of the diamond crystal. It seems plausible that the more disordered structure found in the larger system exhibits a higher entropy but similar energy and packing as "perfect" diamond. We speculate that the entropy gain of partly disordered structures might be less significant in small periodic systems but becomes higher once that clusters can adopt different configurations in adjacent unit cells. It is also worth noting that, different from the primitive porous material in which cavities at the lattice sites were nearly spherical, in the diamond bicontinuous porous materials, the lattice nodes are delimited by surface folds that might favor more disordered structures.

Diamond-like structures have been obtained before in colloidal systems by designing specific isotropic potentials with competing interactions[34,35] and more recently using DNA strands to direct the self-assembly of such structures aiming the development of materials with applications in photonics.[36] However, the structures obtained in the abovementioned works are simple crystals in the sense that each lattice position is occupied by an individual colloidal particle unlike the structure we present here that is composed of clusters.

Next, we investigated the assembly behavior in the diamond porous structure at the same temperature but at a higher chemical potential, corresponding to conditions at which the cylindrical phase is the stable state in bulk. Intuitively, one would expect that the confined fluid can still form a triangular arrangement of cylindrical clusters running through the pores parallel to the face diagonals of the cube ([110] direction). This is indeed what we found in a porous matrix built by setting $L = 20\sigma$ and $n = 2$ at a chemical potential $\mu = -2.175$ (see Figure 6). The distance between nearest cylinders is now

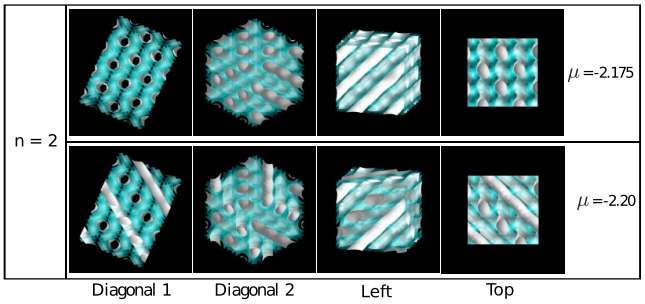

Figure 6. Structures of the confined SALR fluid in porous materials with a diamond structure in thermodynamic conditions at which the hexagonal cylindrical phase is stable in bulk, $T = 0.35$ and $\mu = -2.175$ and -2.20 as indicated. The length of the simulation box edge is $L = 20\sigma$ and contains two unit cells of the porous material ($n = 2$). The gray surface corresponds to the isosurface with local density $\rho_{iso} = 0.4$, and the light blue surface correspond to the pore walls. The average densities are $<\rho> = 0.1877(5),0.1861(4)$, and the average numbers of particles are $<N> = 1502(5),1488(7)$. Four views of the structures are presented.

imposed both by the interaction potential and by the confining material, and in this particular case, the average distance between nearest cylinders is $\sqrt{2}/2 \times L/n = 7.07\sigma$. Cylinders are no longer straight as in bulk; instead, they adopt a sinusoidal shape to adjust to the confining geometry. This cylindrical structure appears to be degenerated with other structures in which cylinders in successive layers are randomly oriented along the possible directions allowed by the confining material. In the example shown in Figure 6, cylinders are parallel to the [110] and [101] directions in alternate layers so that cylinders belonging to two adjacent layers form an angle of $\pi/3$. Both structures exhibit virtually the same energy ($<u> = -3.30$) and the same density ($<\rho> = 0.188$ in the structure in which all the cylinder axes are parallel to each other versus $<\rho> = 0.186$ when cylinders arrange in layers in which cylinders rotate by an angle $\pi/3$). The estimated radius of the cylindrical clusters in both examples is $r_0 = 1.95$, which is quite similar to that found in the primitive porous material (see Figure 3).

Confinement in the G Material. Finally, we consider gyroid porous materials, which are the ones with more complex structures studied in this work. The gyroid porous matrix exhibits channels running along the diagonal of the cube ([111] direction) and along the x-axis ([100] direction), which are interconnected by additional segments so that three channels meet at each junction (8 junctions per unit cell, and $8 \times 3/2 = 12$ connecting segments). The junctions and connecting segments form octagonal helical structures of alternating chirality that are interconnected by porous segments. The porous structures were built by setting the

https://dx.doi.org/10.1021/acs.jpcb.0c08148
J. Phys. Chem. B 2020, 124, 10567−10577

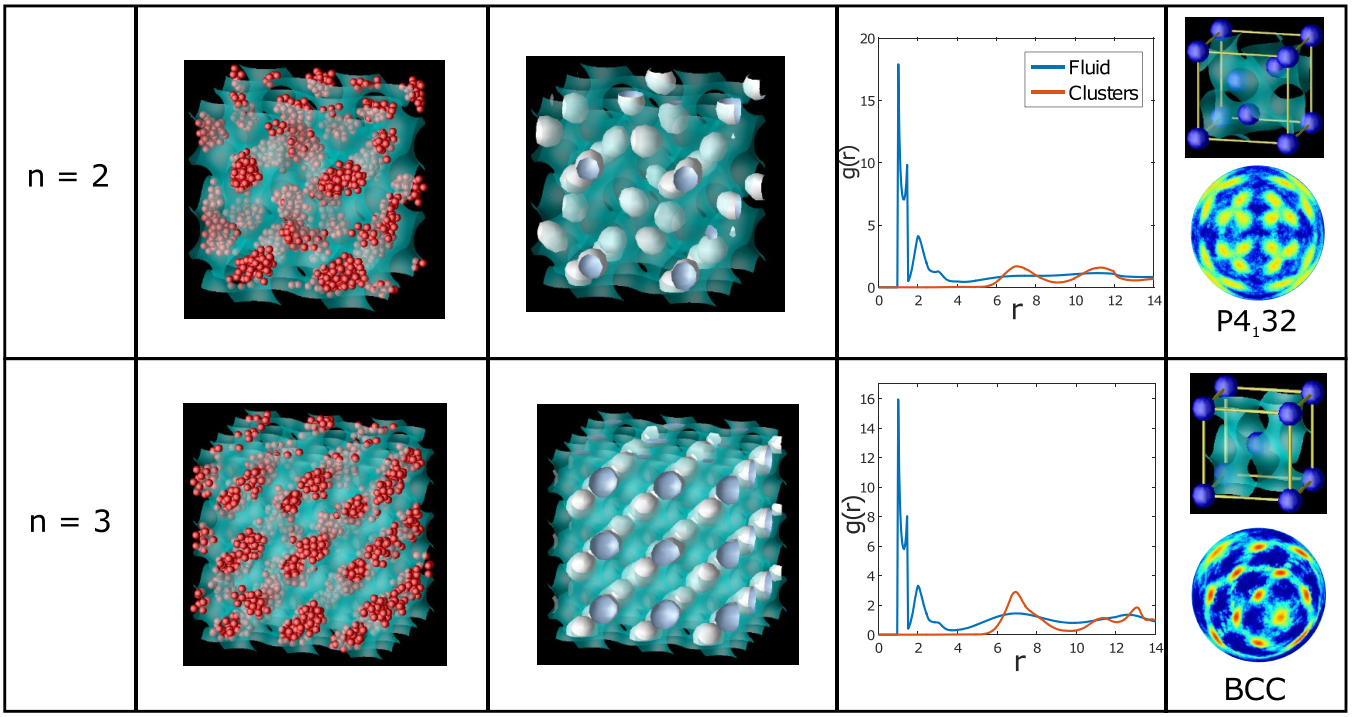

Figure 7. Structures of SALR colloidal particles confined in gyroid porous materials in thermodynamic conditions at which the FCC cluster crystal is the stable phase in bulk (T = 0.35 and μ = − 2.46). The length of the simulation box edge was set to $L = 24\sigma$. In the second column, a snapshot of an equilibrium configuration is shown, and the average local density is presented in the third column. The gray surface corresponds to the isosurface with local density ρ_{iso} = 0.4, and the light blue surface correspond to the pore walls. The average densities are $<\rho>$ = 0.08743(109),0.1148(6) and the average numbers of particles are $<N>$ = 1209(15),1587(7) for n = 2,3, respectively. The fourth column shows the particle−particle and cluster−cluster pair correlation functions, and the fifth column shows the unit cell and BOOD diagram calculated up to first minimum in the cluster−cluster distribution function.

edge length to $L = 24\sigma$. In thermodynamic conditions at which the FCC cluster crystal is the stable phase in bulk (namely, T = 0.35 and μ = − 2.46), we found ordered cluster phases for the porous matrices with n = 2 and n = 3. In the case of n = 2, the clusters are arranged into an ordered structure whose unit cell contains four lattice positions (Figure 7). The clusters are located at the three-channel junctions, but only half the junctions are occupied. After identification of the unit cell with the aid of the density maps of the adsorbed fluid, using the FindSym software,[37,38] we found that this structure exhibits $P4_132$ point group symmetry (space group 213 in crystallographic tables). In this structure, each cluster is surrounded by other six clusters in the first coordination shell at an average distance of roughly 7.35σ and 12 clusters in the second shell at 11.2σ, as revealed by the two first maxima in the cluster−cluster distribution function. The BOOD diagram shows that the structure is orientally ordered, with a very distinctive signature formed by 24 bright spots arranged in clover-shaped groups of three. The emergence of so many bright spots in the BOOD is again caused by the fact that the first coordination shell of each atom in the unit cell is oriented differently from each other.

For the system with n = 3, the clusters are arranged forming a BCC lattice. Clusters are now located at the connecting pores between junctions, but only two per gyroid unit cell are occupied (one per turn of each octagonal helical structure). The average distance between nearest neighbor clusters in this case is about 6.9σ, large enough to avoid significant repulsion between nearest clusters, similar to the other ordered cluster structures found in the P and D porous materials. The second coordination shell that contains six neighbors is located at about 8σ. This is reflected in the cluster−cluster distribution function that shows a rather broad double peak with maxima around these two distances. The BOOD diagram measured with those clusters whose centers of mass are at a distance shorter than the first minimum in the cluster−cluster distribution function exhibits 14 bright peaks, as it is typical of BCC materials.[29] Note that there is a small but non-negligible probability of finding the neighbors at orientations outside these brightest regions, evidencing that clusters are quite mobile in this structure.

At the same temperature and at a higher chemical potential (T = 0.35, μ = − 2.25), at which a triangular lattice of cylindrical clusters is stable in bulk, we could only obtain ordered structures for the porous material with n = 3. In this case, the confined fluid organizes into approximately cylindrical clusters arranged into a triangular lattice with the cylinders running along the cube diagonal as shown in Figure 8. The cylinders are not completely straight, again showing a sinusoidal shape to adapt to the pore geometry. The average distance between nearest cylinders is imposed by the confining material. Six cylinders are formed along the cube diagonal so that the distance between nearest cylinders is $\sqrt{3} \times L/6 = 6.93\sigma$. The estimated equilibrium radius is r_0 = 2.05σ, of the same order of the cylindrical phases found in the other confining materials.

The Effect of Temperature. Once we have identified the stable ordered structures in the different porous materials, we wonder whether these microphases become locally ordered at low temperature. To answer this question, we perform

https://dx.doi.org/10.1021/acs.jpcb.0c08148
J. Phys. Chem. B 2020, 124, 10567−10577

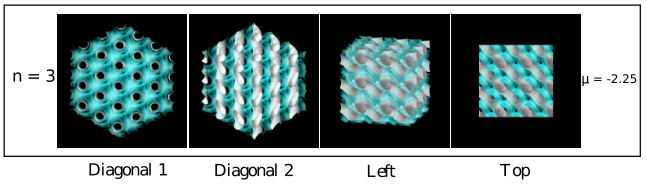

Figure 8. Structure of SALR particles confined in gyroidal pores built by setting $L = 24\sigma$ and $n = 3$ in thermodynamic conditions at which the cylindrical phase is the stable state in bulk ($T = 0.35$, $\mu = -2.25$). The gray surface corresponds to the isosurface with local density $\rho_{iso} = 0.4$, and the light blue surface correspond to the pore walls. The average density is $<\rho> = 0.1817(4)$, and the average number of particles is $<N> = 2511(5)$. Four views of the structures are presented.

simulations in the grand canonical ensemble at the same chemical potential at which cluster crystals were found to be stable in the previous section, while the temperature is varied in the range $0.25 \leq T \leq 0.55$. Note that all the cluster crystal phases are expected to be stable at low temperature, but the range of stability shifts to lower chemical potential as temperature decreases. However, internal ordering of the clusters might only occur at low temperature for the upper limit of densities for which cluster crystals are stable. We try to reach those thermodynamic conditions by performing a quench at constant chemical potential.

As expected, at low temperatures, the amount of adsorbed particles increases. However, in many cases, this leads to the formation of elongated clusters that grow through the cavities of the material linking the lattice nodes of the original structure. On the other hand, as the temperature is increased, the desorption is favored and the cluster size decreases until the structure melts into a cluster-fluid. However, as can be seen in Figure 9, there are differences between the different cluster

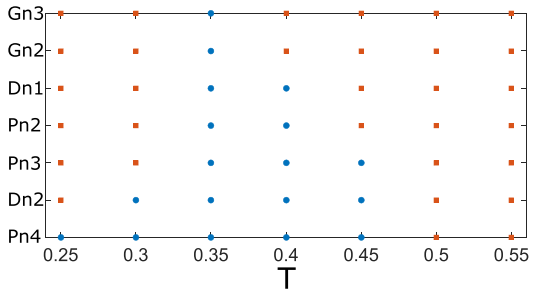

Figure 9. Temperature stability scheme of the cluster crystals obtained under confinement in the porous materials. The states where the structure is not stable are represented with red squares, and the states of stability are represented with blue circles. The structures are ordered from the most stable (bottom) to the less stable(top).

crystals. Rather unsurprisingly, the FCC is the most stable phase, whereas those stabilized in the G material are the less stable.

Interestingly, the FCC cluster crystal formed in the D material ($n = 2$) is less stable than the one templated with the P matrix ($n = 4$). In the P material, the clusters are located at alternate spherical cavities that act as strong nucleation sites. Additionally, the necks connecting the cavities are too narrow ($D_{neck}/\sigma \approx 3.0$) for the clusters to grow through them. Thus, the system can achieve a better packing by rearrangement of the clusters in the spherical cavities. On the contrary, in the D material, cavities at the lattice nodes are connected along the face diagonals of the simulation box by pores of comparable dimension to the lattice cavities, favoring that adjacent clusters can merge as temperature decreases (thus increasing density).

The fact that the FCC in the P material is able to survive at $T = 0.25$ by improving the packing inside the cavities must be accompanied by a rearrangement of the particles within the clusters. In Figure 10, we present the results of the effect of the

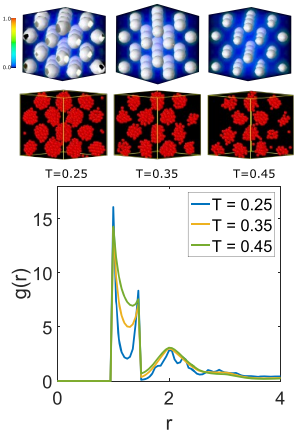

Figure 10. Effect of temperature on the FCC cluster crystal obtained for the material P with $n = 4$. The walls of the porous material are not shown to better visualize the effect of the temperature on the local structure of the system.The top panels show the local density maps, and the isosurfaces with $\rho_{iso} = 0.4$ are plotted. The central panels show equilibrium snapshots. The bottom panel shows the pair correlation functions of the colloidal particles. The average density is $<\rho> = 0.1960(26),0.1259(3),0.0767(27)$ and the average number of particles is $<N> = 1568(21),1007(3),613(22)$ for the temperature $T = 0.25,0.35,0.45$, respectively.

temperature on such a structure. From the density maps, we observe that as the temperature increases, the size of the clusters decreases, as expected. On the contrary, at low temperature, the size increases, reflecting the higher density. Interestingly, particles within the clusters become often ordered forming a stacking of triangular layers. The building up of intracluster ordering is reflected in the particle−particle distribution function at $T = 0.25$. The two first peaks are sharper, and the third and fourth peaks are now split in additional smaller but clearly visible peaks (see Figure 10). The presence of crystalline-like microphases has already been reported previously,[39−41] and it seems to be a common feature of colloidal systems interacting via potentials with a clear minimum in the attractive range. Since the square-well-linear potential has a flat attractive interaction, solid-like microphases are not often found, although it might appear at very low temperature.[2,3,21] Our results show that confinement can be used to promote local ordering in microphases.

SUMMARY AND CONCLUSIONS

In this work, we investigated the possibility of using porous materials with ordered structures as three-dimensional templates to direct the self-assembly of colloidal fluids with competing interactions into ordered microphase structures that might be potentially useful in nanotechnology. Using grand canonical Monte Carlo simulations, we investigated the assembly of an SALR fluid in porous materials with primitive,

https://dx.doi.org/10.1021/acs.jpcb.0c08148
J. Phys. Chem. B 2020, 124, 10567−10577

diamond, and gyroid structures, using the pore size as another independent variable.

We found that indeed these porous materials can be used to control the structure of the adsorbed fluid. For a given porous structure and at chemical potentials at which the cluster crystal is the stable phase in bulk, different cluster crystals can be obtained by varying the size of the porous unit cell so that both the pore size and distance between pores change. Besides obtaining cluster crystals with the same structure as the confining material (in the case of P and D porous materials, albeit with some defects in the latter case), we found that it is also possible to obtain cluster crystals with a different structure by tuning the unit cell of the porous material. If the unit cell is so big that the distance between nearest lattice sites becomes too large compared to the interaction range, cluster crystals form by occupying the connecting segments between the lattice sites. On the contrary, if the porous unit cell is too small compared with the interaction range, cluster crystals form by occupying a sublattice for which the nearest neighbor sites achieve a better compromise between avoiding repulsion interactions and efficient packing. Interestingly, we were able to stabilize open structures that are often difficult to achieve using isotropic units but that are particularly appealing for applications.

By setting a higher chemical potential, at which the cylindrical phase is stable in bulk, the absorbed fluid can also adopt different configurations from that found in bulk. Besides having certain control over the distance between cylinders, it is also possible to obtain stacking of layers of cylinders with different orientations.

Despite considerable effort, ordered cluster phases formed by colloids with competing interactions have not been experimentally observed.[42,43] Our results suggest that a possible route to obtain such ordered microphases is to use three-dimensional porous materials as templates. The reduced configurational space might possibly promote the formation of ordered microphases with less interference from dynamically arrested states as in bulk.[44−47] The regular porous structure enhances the formation, ordering, and stability of clusters. We may speculate that the time necessary to form a well-ordered cluster crystal may depend on the sizes of the pores and their connectivity. The diffusion of the molecules in confined geometry may be slower than that in bulk. It may result in kinetically arrested states, but once the order structure is formed, it should be more stable than the ordered structure in bulk.

AUTHOR INFORMATION

Corresponding Author

Wojciech T. Góźdź − *Institute of Physical Chemistry, Polish Academy of Sciences, 01-224 Warsaw, Poland;* orcid.org/0000-0003-4506-6831; Email: wtg@ichf.edu.pl

Authors

Horacio Serna − *Institute of Physical Chemistry, Polish Academy of Sciences, 01-224 Warsaw, Poland*

Eva G. Noya − *Instituto de Química Física Rocasolano, CSIC, 28006 Madrid, Spain;* orcid.org/0000-0002-6359-1026

Complete contact information is available at: https://pubs.acs.org/10.1021/acs.jpcb.0c08148

Notes

The authors declare no competing financial interest.

ACKNOWLEDGMENTS

We would like to thank A. Ciach for helpful discussion and support of our work. This publication is part of a project that has received funding from the European Union's Horizon 2020 research and innovation programme under the Marie Skłodowska-Curie grant agreement No. 711859 to H.S. and No. 734276 to H.S and W.T.G. Additional funding was received from the Ministry of Science and Higher Education of Poland for the project No. 734276 in the years 2017-2018 (agreement No. 3854/H2020/17/2018/2) and for the implementation of the international co-financed project No. 711859 in the years 2017-2021. We would like to acknowledge the support from NCN, Grant No 2015/19/B/ST3/03122 and Grant No 2018/30/Q/ST3/00434 and from the Agencia Estatal de Investigación and the Fondo Europeo de Desarrollo Regional (FEDER), Grant No FIS2017-89361-C3-2-P.

REFERENCES

(1) Sweatman, M. B.; Fartaria, R.; Lue, L. Cluster formation in fluids with competing short-range and long-range interactions. *J. Chem. Phys.* **2014**, *140*, No. 03B626_1.

(2) Zhuang, Y.; Charbonneau, P. Recent advances in the theory and simulation of model colloidal microphase formers. *J. Phys. Chem. B* **2016**, *120*, 7775−7782.

(3) Zhuang, Y.; Zhang, K.; Charbonneau, P. Equilibrium phase behavior of a continuousspace microphase former. *Phys. Rev. Lett.* **2016**, *116*, No. 098301.

(4) Mann, S. Self-assembly and transformation of hybrid nano-objects and nanostructures under equilibrium and non-equilibrium conditions. *Nat. Mater.* **2009**, *8*, 781.

(5) Whitesides, G. M.; Grzybowski, B. Self-Assembly at All Scales. *Science* **2002**, *295*, 2418−2421.

(6) Grzelczak, M.; Vermant, J.; Furst, E. M.; Liz-Marzán, L. M. Directed self-assembly of nanoparticles. *ACS Nano* **2010**, *4*, 3591−3605.

(7) Yin, Y.; Lu, Y.; Gates, B.; Xia, Y. Template-assisted self-assembly: a practical route to complex aggregates of monodispersed colloids with well-defined sizes, shapes, and structures. *J. Am. Chem. Soc.* **2001**, *123*, 8718−8729.

(8) Doerk, G. S.; Yager, K. G. Beyond native block copolymer morphologies. *Mol. Syst. Des. Eng.* **2017**, *2*, 518−538.

(9) Wu, Y.; Cheng, G.; Katsov, K.; Sides, S. W.; Wang, J.; Tang, J.; Fredrickson, G. H.; Moskovits, M.; Stucky, G. D. Composite mesostructures by nano-confinement. *Nat. Mater.* **2004**, *3*, 816.

(10) Bai, P.; Yang, S.; Bao, W.; Kao, J.; Thorkelsson, K.; Salmeron, M.; Zhang, X.; Xu, T. Diversifying Nanoparticle Assemblies in Supramolecule Nanocomposites Via Cylindrical Confinement. *Nano Lett.* **2017**, *17*, 6847−6854.

(11) Bianchi, E.; Likos, C. N.; Kahl, G. Self-assembly of heterogeneously charged particles under confinement. *ACS Nano* **2013**, *7*, 4657−4667.

(12) Serna, H.; Noya, E. G.; Góźdź, W. T. Assembly of helical structures in systems with competing interactions under cylindrical confinement. *Langmuir* **2018**, *35*, 702−708.

(13) Serna, H.; Noya, E. G.; Góźdź, W. T. The influence of confinement on the structure of colloidal systems with competing interactions. *Soft Matter* **2020**, *16*, 718−727.

(14) Shi, A.-C.; Li, B. Self-assembly of diblock copolymers under confinement. *Soft Matter* **2013**, *9*, 1398−1413.

(15) Bores, C.; Almarza, N. G.; Lomba, E.; Kahl, G. Inclusions of a two dimensional fluid with competing interactions in a disordered, porous matrix. *J. Phys.: Condens. Matter* **2015**, *27*, 194127.

(16) Qiao, C. Z.; Zhao, S. L.; Liu, H. L.; Dong, W. Connect the Thermodynamics of Bulk and Confined Fluids: Confinement-Adsorption Scaling. *Langmuir* **2019**, *35*, 3840−3847.

(17) Lima, E. O.; Pereira, P. C. N.; Löwen, H.; Apolinario, S. W. S. Complex structures generated by competing interactions in

harmonically confined colloidal suspensions. *J. Phys.: Condens. Matter* **2018**, *30*, 325101.
(18) Pinge, S.; Lin, G.; Baskaran, D.; Padmanaban, M.; Joo, Y. L. Designing an ordered template of cylindrical arrays based on a simple flat plate confinement of block copolymers: a coarse-grained molecular dynamics study. *Soft Matter* **2018**, *14*, 597−613.
(19) Wang, C.; Zhao, Y.; Zhou, L.; Liu, Y.; Zhang, W.; Zhao, Z.; Hozzein, W. N.; Alharbi, H. M. S.; Li, W.; Zhao, D. Mesoporous carbon matrix confinement synthesis of ultrasmall WO_3 nanocrystals for lithium ion batteries. *J. Mater. Chem. A* **2018**, *6*, 21550−21557.
(20) Zhao, J.; Yin, Y.; Li, Y.; Chen, W.; Liu, B. Synthesis and characterization of mesoporous zeolite Y by using block copolymers as templates. *Chem. Eng. J.* **2016**, *284*, 405−411.
(21) Zhuang, Y.; Charbonneau, P. Equilibrium phase behavior of the square-well linear microphase-forming model. *J. Phys. Chem. B* **2016**, *120*, 6178−6188.
(22) Campbell, A. I.; Anderson, V. J.; van Duijneveldt, J. S.; Bartlett, P. Dynamical arrest in attractive colloids: The effect of long-range repulsion. *Phys. Rev. Lett.* **2005**, *94*, 208301.
(23) Sciortino, F.; Tartaglia, P.; Zaccarelli, E. One-dimensional cluster growth and branching gels in colloidal systems with short-range depletion attraction and screened electrostatic repulsion. *J. Phys. Chem. B* **2005**, *109*, 21942−21953.
(24) Banerjee, D.; Lindquist, B. A.; Jadrich, R. B.; Truskett, T. M. Assembly of particle strings via isotropic potentials. *J. Chem. Phys.* **2019**, *150*, 124903.
(25) Schoen, A. H. *NASA Report No. TN D-5541*.
(26) Allen, M. P.; Tildesley, D. J. *Computer simulation of liquids*; Oxford university press, 2017.
(27) Deserno, M. Available from: https://www.cmu.edu/biolphys/deserno/pdf/gr_periodic.pdf.
(28) Dawass, N.; Krüger, P.; Schnell, S. K.; Bedeaux, D.; Kjelstrup, S.; Simon, J. M.; Vlugt, T. J. H. Finite-size effects of Kirkwood−Buff integrals frommolecular simulations. *Mol. Simul.* **2018**, *44*, 599−612.
(29) Spellings, M.; Glotzer, S. C. Machine learning for crystal identification and discovery. *AIChE J.* **2018**, *64*, 2198−2206.
(30) Góźdź, W. T.; Hołyst, R. Triply periodic surfaces and multiply continuous structures from the Landau model of microemulsions. *Phys. Rev. E* **1996**, *54*, 5012−5027.
(31) Rocklin, D. Z.; Mao, X. Self-assembly of three-dimensional open structures using patchy colloidal particles. *Soft Matter* **2014**, *10*, 7569.
(32) Reinhart, W. F.; Panagiotopoulos, A. Z. Equilibrium crystal phases of triblock Janus colloids. *J. Chem. Phys.* **2016**, *145*, No. 094505.
(33) Pattabhiraman, H.; Avvisati, G.; Dijkstra, M. Novel pyrochlore-like crystal with a photonic band gap self-assembled using colloids with a simple interaction potential. *Phys. Rev. Lett.* **2017**, *119*, 157401.
(34) Marcotte, É.; Stillinger, F. H.; Torquato, S. Communication: Designed diamond ground state via optimized isotropic monotonic pair potentials. *J. Chem. Phys.* **2013**, No. 061101.
(35) Jain, A.; Errington, J. R.; Truskett, T. M. Dimensionality and design of isotropic interactions that stabilize honeycomb, square, simple cubic, and diamond lattices. *Phys. Rev. X* **2014**, *4*, No. 031049.
(36) Wang, Y.; Jenkins, I. C.; McGinley, J. T.; Sinno, T.; Crocker, J. C. Colloidal crystals with diamond symmetry at optical lengthscales. *Nat. Commun.* **2017**, *8*, 14173.
(37) Stokes, H. T.; Hatch, D. M.; Campbell, B. J. *FINDSYM, ISOTROPY Software Suite*. iso.byu.edu
(38) Stokes, H. T.; Hatch, D. M. Program for Identifying the Space Group Symmetry of a Crystal. *J. Appl. Crystallogr.* **2005**, *38*, 237.
(39) De Candia, A.; Del Gado, E.; Fierro, A.; Sator, N.; Tarzia, M.; Coniglio, A. Columnar and lamellar phases in attractive colloidal systems. *Physical Review E* **2006**, *74*, No. 010403.
(40) Coniglio, A.; de Candia, A.; Fierro, A. Modulated phases and structural arrest in colloidal systems with competing interactions. *Mol. Phys.* **2011**, *109*, 2981−2987.
(41) Pękalski, J.; Rządkowski, W.; Panagiotopoulos, A. Z. Shear-induced ordering in systems with competing interactions: A machine learning study. *J. Chem. Phys.* **2020**, *152*, 204905.
(42) Royall, C. P. Hunting mermaids in real space: Known knowns, known unknowns and unknown unknowns. *Soft Matter* **2018**, *14*, 4020−4028.
(43) Guo, Y.; van Ravensteijn, B. G. P.; Kegel, W. K. Self-assembly of isotropic colloids into colloidal strings, Bernal spiral-like, and tubular clusters. *Chem. Commun.* **2020**, *56*, 6309−6312.
(44) Zhuang, Y.; Charbonneau, P. Communication: Microphase equilibrium and assembly dynamics. *J. Chem. Phys.* **2017**, *147*, No. 091102.
(45) Stopper, D.; Roth, R. Nonequilibrium phase transitions of sheared colloidal microphases: Results from dynamical density functional theory. *Phys. Rev. E* **2018**, *97*, No. 062602.
(46) Ruiz-Franco, J.; Jaramillo-Cano, D.; Camargo, M.; Likos, C. N.; Zaccarelli, E. Multiparticle collision dynamics for a coarse-grained model of soft colloids. *J. Chem. Phys.* **2019**, *151*, No. 074902.
(47) Klix, C. L.; Royall, C. P.; Tanaka, H. Structural and dynamical features of multiple metastable glassy states in a colloidal system with competing interactions. *Phys. Rev. Lett.* **2010**, *104*, 165702.

https://dx.doi.org/10.1021/acs.jpcb.0c08148
J. Phys. Chem. B 2020, 124, 10567−10577